Geology, Geochemistry, and Geochronology (U-Pb) of the Rio Fortuna Gneiss – Serra do Baú Intrusive Suite – Paraguá Terrane – SW Amazonian Craton

Geologia, Geoquímica e Geocronologia (U-Pb) do Gnaisse Rio Fortuna – Suíte Intrusiva Serra do Baú – Terreno Paraguá – SO do Cráton Amazônico

Débora Almeida Faria[1,2]*, **Amarildo Salina Ruiz[1,2,3]**, **João Batista Matos[1,2,4]**, **Maria Zélia Aguiar de Sousa[1,2,4]**, **Gabrielle Aparecida de Lima[1,2]**, **Moacir José Buenano Macambira[1,5]**

RESUMO: O Gnaisse Rio Fortuna aflora na região da serra Santa Bárbara, nas imediações do Destacamento Militar Fortuna, na fronteira Brasil–Bolívia. Estes ortognaisses estão inseridos no Terreno Paraguá, em um setor afetado pela Orogenia Sunsás (1.0 a 0.9 Ga.). São classificados como ortognaisses de composição monzo a granodiorítica, com registros de, no mínimo, três fases de deformação. Idade U-Pb em zircão de 1.711 ± 13 Ma obtida por ablação a laser MC-ICP-MS, é considerada como correspondendo à idade de cristalização do protólito ígneo. Geoquimicamente, essas rochas constituem uma sequência ácida formada por um magmatismo subalcalino, do tipo cálcio-alcalino de alto potássio, metaluminoso a peraluminoso.

PALAVRAS-CHAVE: *Cráton Amazônico; geologia estrutural; geoquímica; geocronologia U-Pb.*

ABSTRACT: *The Rio Fortuna Gneiss crops out in the Serra Santa Barbara, near the Fortuna military headquarters, on the Brazil–Bolivia border. These orthogneisses are located in a portion of the Paraguá terrain affected by the Sunsás Orogeny (1.0–0.9 Ga.). They are classified as monzo to granodiorite orthogneisses and underwent at least three episodes of deformation. The U-Pb zircon age of 1,711 ± 13 Ma obtained by laser ablation MC-ICP-MS is interpreted as the crystallization age of this orthogneiss. Geochemically, these rocks form a sequence comprising acidic subalkaline magmatism, calc-alkalic-type high-K, and metaluminous to peraluminous.*

KEYWORDS: *Amazonian Craton; structural geology; geochemistry; U-Pb geochronology.*

INTRODUCTION

The SW portion of the Amazonian Craton that crops out in Mato Grosso is part of the Rondonian-San Ignácio Geochronological Province. It holds geological and tectonic records of successive continental accretions, from the paleo- to the neoproterozoic. These successive accretion processes resulted in the juxtaposition of allochthonous terrains (Saes 1999; Geraldes 2000; Boger *et al.* 2005; Ruiz 2005), which have been recently redefined by Ruiz (2009) and Bettencourt *et al.* (2010) as follows: Jauru Terrane (1.78 – 1.42 Ga.), Alto Guaporé Terrane (1.42 – 1.34 Ga.), Rio Alegre Terrane (1.51 – 1.38 Ga.), and Paraguá Terrane (1.82 – 1.32 Ga.).

Litherland *et al.* (1986) recognized three lithostratigraphic units that were formed prior to the onset of the San Ignácio and Sunsás orogenies. These units make up the Bolivian

[1]Research Group on Crustal and Tectonic Evolution, Guaporé (RS), Brazil. *E-mail: defaal.debora@gmail.com; gabilimagel@gmail.com; asruiz@gmail.com; jmatos@ufmt.br; prof.mzaguiar@gmail.com; moamac@ufpa.br*

[2]Post-Graduate Program in Geosciences, *Instituto de Ciências Exatas e da Terra -ICET, Universidade Federal de Mato Grosso* - UFMT, Cuiabá (MT), Brazil. *Instituto Nacional de Ciência e Tecnologia de Geociências da Amazônia* - GEOCIAM, Belém (PA), Brazil.

[3]Department of General Geology, *Instituto de Ciências Exatas e da Terra* - ICET, *Universidade Federal de Mato Grosso* - UFMT, Cuiabá (MT), Brazil.

[4]Department of Mineral Resources, *Instituto de Ciências Exatas e da Terra* - ICET, *Universidade Federal de Mato Grosso* - UFMT, Cuiabá (MT), Brazil.

[5]Pará-Iso Laboratory of Geochronology, *Universidade Federal do Pará* - UFPA, Belém (PA), Brazil.

*Corresponding author

Manuscrito ID: 30024. **Recebido em:** 27/08/2013. **Aprovado em:** 03/02/2014

paleoproterozoic basement and have the following characteristics: the Lomas Manechis Granulitic Complex, which is composed of enderbitic charnockites and feldspathic quartz-banded gneiss; the Chiquitania Gneiss Complex, which consists mainly of orthogneiss (Division B) and paragneiss (Division A), and the San Ignácio Schist Supergroup, which consists of an association of sedimentary metavolcanic rocks.

In Brazil, narrow granulitic bands (most likely associated with the Lomas Manechis Granulitic Complex) were found (Matos *et al.* 2006), in addition to several banded orthogneiss bodies, which were grouped by Ruiz (2005) in the Serra do Baú Intrusive Suite (SBIS) and correlated to the gneisses in Division B of Litherland *et al.*(1986).

The Rio Fortuna Gneiss, which is this study's object, was defined as part of the Chiquitania Gneiss Complex by Litherland *et al.* (1986) and geochronologically studied by Santos *et al.* (2008), who published U-Pb zircon ages of approximately 1,336 ± 3 Ma as the crystallization age for the igneous protolith, whereas values between 1,772 and 1,734 Ma were interpreted as the inheritance.

Based on a lithostructural mapping, followed by geochemical and petrographic analyses and U-Pb zircon dating of the Rio Fortuna Gneiss, this study intends to elucidate the magmatic and tectono-metamorphic evolution of the orthogneiss units in the SBIS, Paraguá Terrane, Rondonian-San Ignácio Province.

REGIONAL GEOLOGICAL CONTEXT

The Amazonian Craton is surrounded by neoproterozoic orogenic belts and is divided into six large geochronological provinces: Central Amazonian (> 2.3 Ga.), Maroni-Itacaiúnas (2.2 – 1.95 Ga.), Ventuari-Tapajós (1.95 – 1.80 Ga.), Rio Negro-Juruena (1.8 – 1.55 Ga.), Rondoniana-San Ignácio (1.55 – 1.3 Ga.), and Sunsás (1.3 – 1.0 Ga.) (Teixeira *et al.* 1989; Tassinari & Macambira 1999; Santos *et al.* 2000; Tassinari *et al.* 2000). Ruiz (2005) further adds the Rio Apa Province (1.8 – 1.3 Ga.) to the partitioning proposed by Tassinari *et al.* (2000), thus extending the Amazonian Craton south from the Tucavaca Aulacogen (Fig. 1A). Santos *et al.* (2000 and 2008) propose a different craton partitioning, and according to these authors, the area studied herein is located within the Sunsás Province (1.45 – 1.10 Ga.).

The SW portion of the Amazonian Craton that crops out to the east of Bolivia and part of the states of Rondônia, Mato Grosso, and Mato Grosso do Sul is divided into terrains that, according to Bettencourt *et al.* (2010), are named as follows: Jauru Terrane, Alto Guaporé Terrane, Rio Alegre Terrane, and Paraguá Terrane (Fig. 1B).

The Paraguá Terrane (1.82 – 1.3 Ga.), where the unit under investigation is located, is characterized by a lithotectonic framework formed over at least three orogenic events: Lomas Manechis Orogeny (1.74 – 1.69 Ga.), San Ignácio Orogeny (1.35 – 1.3 Ga.), and Sunsás Orogeny (1.30 – 1.00 Ga.) (Bettencourt *et al.* 2010).

Litherland *et al.* (1986) partitioned the Bolivian portion of the Paraguá Terrane into three lithostratigraphic units: the Lomas Manechis Complex (1.68 Ga.), the San Ignácio Schist Supergroup (< 1.76 Ga.), and the Chiquitania Gneiss Complex. Santos *et al.* (2008) reported the following ages for the Rio Fortuna Gneiss, obtained using the U-Pb zircon dating method: values in the range of 1,772 – 1,734 Ma for the core, which is interpreted as the inheritance, and the value 1,336 ± 3 Ma, found at the rim of the crystal, which is interpreted as the age of protolith formation.

The Brazilian portion of the Paraguá Terrane is characterized by the physical continuity of these main units described for the Bolivian portion. However, the vast occurrence of granulite terrains and the metasedimentary units belonging to the San Ignácio Schist Supergroup are not found in Brazil. In terms of the lithostratigraphic correlation of gneiss units, the Division A gneisses of the Chiquitania Gneiss Complex (Litherland *et al.* 1986) have been correlated to the SBIS bodies described by Ruiz (2005), Faria (2011), and Figueiredo *et al.* (2013).

The SBIS in the region of the Fortuna military headquarters consists of four gneissic bodies, which can be observed in Fig. 2 and are named as follows: Córrego Retiro Gneiss, Córrego Vermelho Gneiss, Córrego Retiro II Gneiss, and Rio Fortuna Gneiss (Faria 2011).

GEOLOGY AND PETROGRAPHY

The Rio Fortuna Gneiss crops out mainly in slabs and blocks, is in tectonic contact with the Tarumã Granite, and is mainly covered by quaternary sediments of the Pantanal Formation. The petrographic study allowed for characterizing the rocks in the Rio Fortuna Gneiss as Biotite Gneiss with titanite, which are classified as granodiorites and monzogranites in Streckeisen's (1976) QAP diagram. The gneiss displays a whitish-gray color, a fine-to-medium grain size, and alternating discontinuous mafic and felsic bands, which are folded or complexly refolded and display granulite xenoliths attributed to the Lomas Manechis Granulitic Complex (Fig. 3).

Optically, the rocks studied herein exhibit a granolepidoblastic texture with gneiss bands defined by beds of quartz and feldspar and millimeter-sized mafic levels composed of biotite, chlorite, and titanite. The accessory minerals are titanite, rutile, allanite, apatite, and opaques, whereas chlorite, titanite, sericite, muscovite, epidote/clinozoisite, clay minerals, calcite, and opaques constitute the alteration
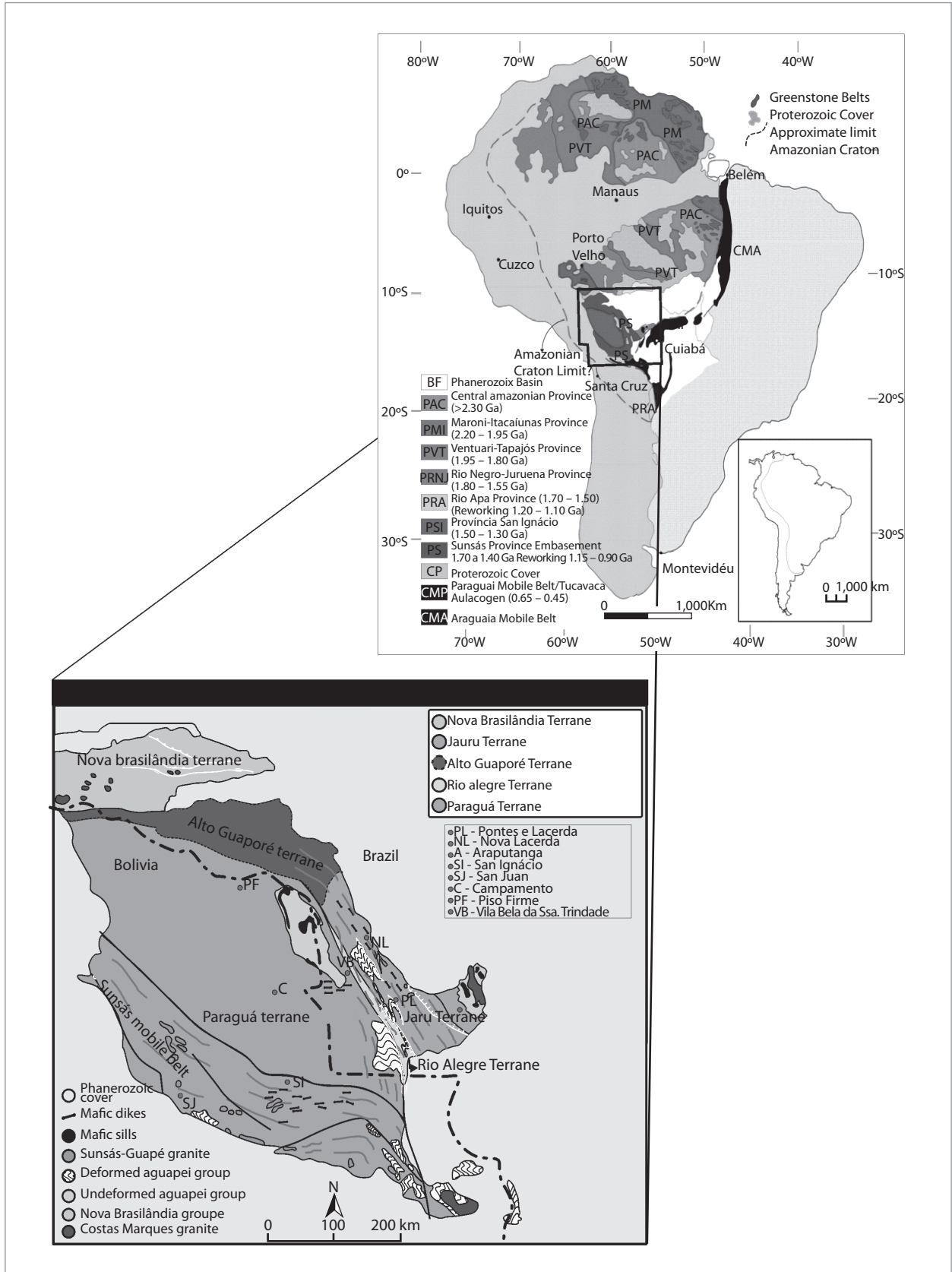
Figure 1. (A) presents a map with the geochronological partitioning of the Amazonian Craton, obtained from Ruiz (2005), and (B) shows the terrain-partitioning map for the SW portion of the Amazonian Craton, obtained from Ruiz (2009).
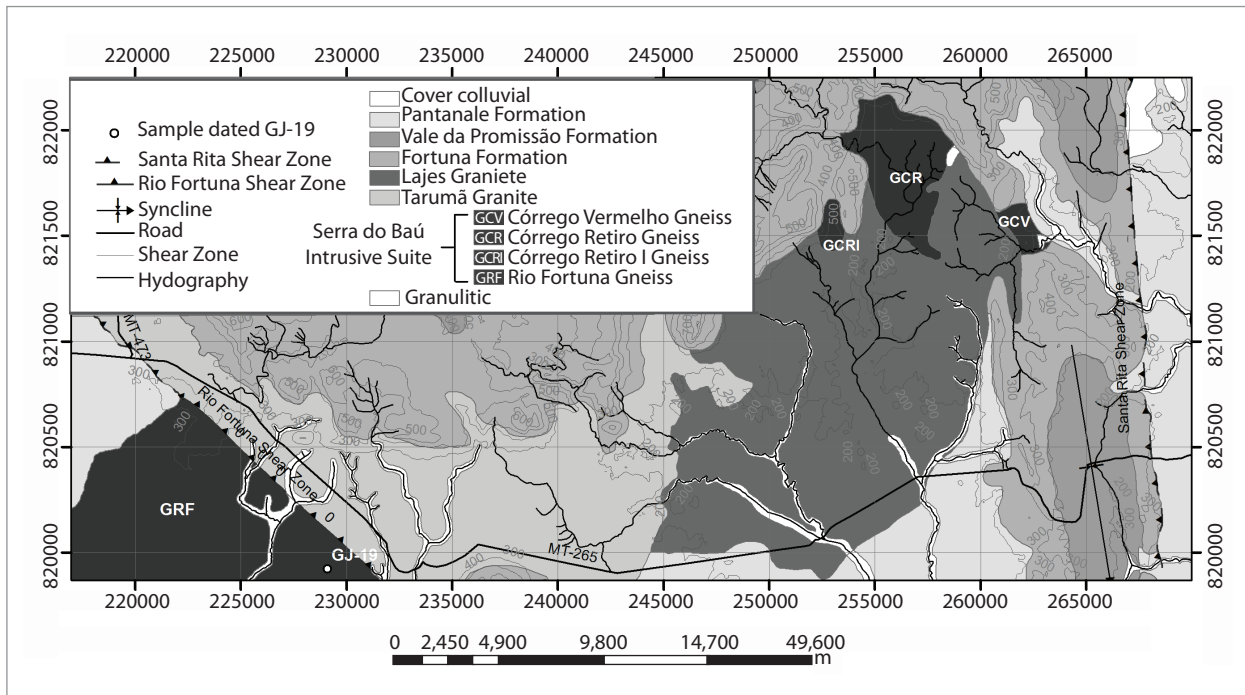
Figure 2. Geological map of Santa Rita region, Brazil-Bolivia border. Highlighting the Gneiss Intrusive Suite Serra do Baú and adjacent units.
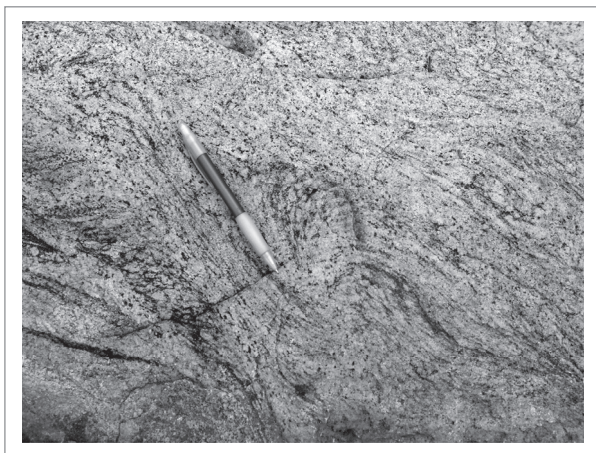

Figure 3. Features of the Rio Fortuna Gneiss: mode of occurrence and field aspect, hand specimen with details of the gneissic banding.

paragenesis. The plagioclase exhibits anhedral and subhedral grains (sometimes shattered, with albite and/or pericline polysynthetic twins) and is classified as oligoclase by the Michel-Levy statistical method. It is locally intergrown with quartz of a vermicular aspect and alkaline feldspar, forming myrmekitic (Fig. 4A) and anti-perthitic textures, respectively, in which the host phase (microcline) is arranged in either a porphyritic form or in lamellae and grains (Fig. 4B). In some samples, it is intensely cloudy due to post-magmatic processes such as sericitization and saussuritization, with large

amounts of epidote/clinozoisite and sericite. The alkaline feldspars occur in anhedral porphiroclasts with shattered edges, found both in microcline and in orthoclase with grid (combined albite + pericline) and Carlsbad twinning, respectively. Commonly, they exhibit intergrowths with quartz that characterize a graphic texture and alteration to sericite and clay minerals. Quartz is found in anhedral grains (sometimes vermicular) in polygonal crystals, creating a mosaic texture and displaying undulatory extinction, dynamic recrystallization, and deformation bands and lamellae (Fig. 4C). Two varieties of primary biotite are found: one in millimeter-sized subhedral needles, with light-brown and greenish-yellow pleochroism, sometimes in a *kink band*, from partially to fully altered to chlorite, and others in thicker lamellae of reddish-brown to dark-green pleochroism, with rutile inclusions characterizing a sagenitic texture (Fig. 4D). Titanite is the most common accessory mineral in these rocks, but it also occurs as a secondary phase. In the first case, it is found in isolation or associated with biotite in the mafic levels or, more rarely, in the felsic bands, where it forms small prismatic crystals (Fig. 4E). As the secondary phase, titanite occurs in anhedral poikiloblasts, constituting a corona that results from an opaque mineral alteration process (possibly from ilmenite). Allanite is another primary episode, sometimes found metamictized with an epidote corona (Fig. 4F). Other accessory minerals are rutile and apatite, both of acicular habit, embedded in biotite and feldspars, respectively; there is also zircon, which
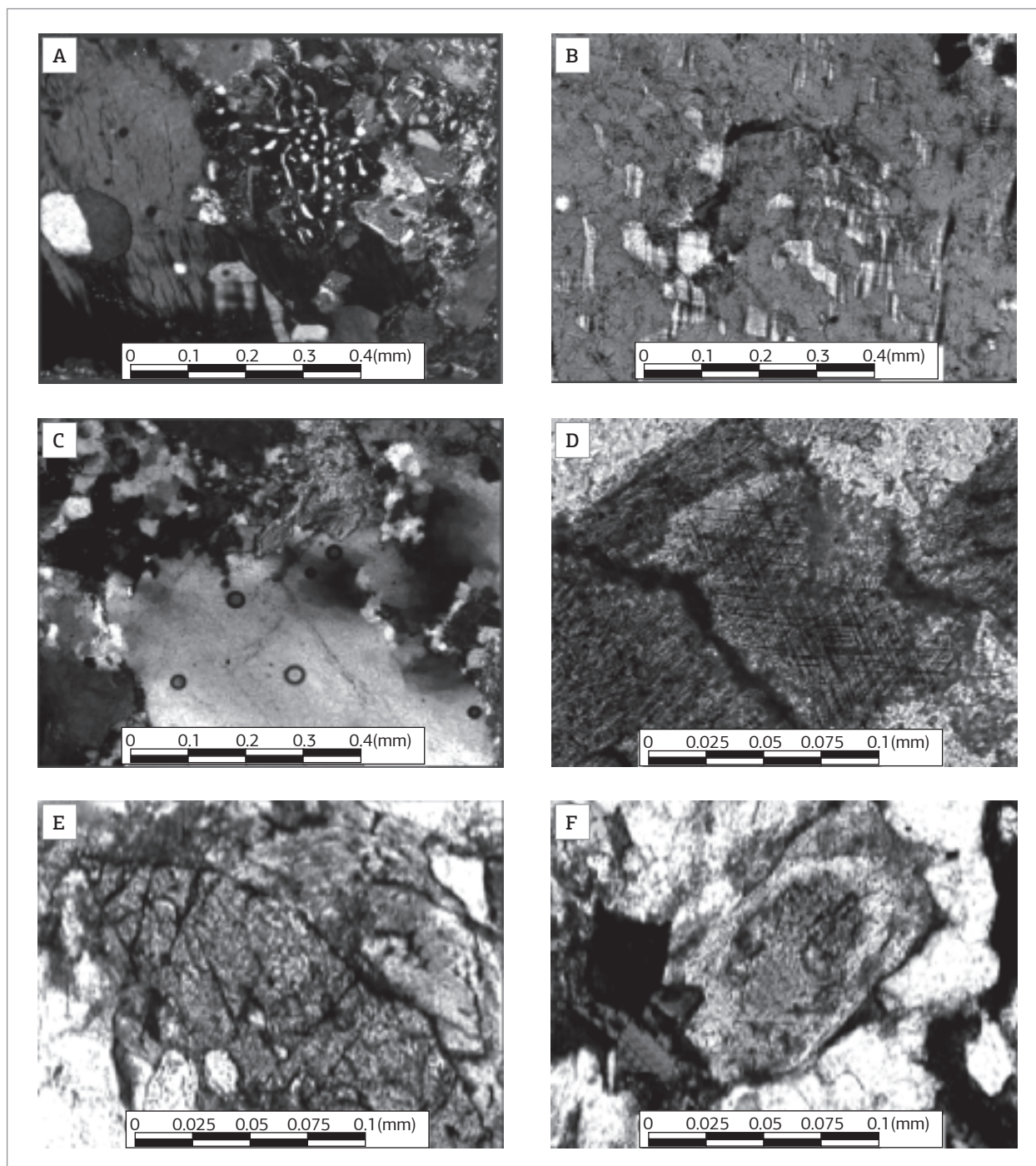
Figure 4. Photomicrograph of the Rio Fortuna Gneiss: (A) myrmekitic intergrowth; (B) anti-perthite detail in which the host phase corresponds to the microcline; (C) recrystallized quartz; (D) biotite with rutile inclusions characterizing a sagenitic texture; (E) primary prismatic titanite crystal associated with biotite; and (F) detail of metamictic allanite with epidote corona.

occurs as tiny crystals dispersed among the felsics or associated with biotite, where the crystals develop pleochroic halos. The opaques constitute primary or alteration phases and are found in crystals ranging from euhedral to anhedral, black or reddish in color, and can be observed interleaved with the mafics, in a symplectic texture, or with opaques, partially altered — thus originating titanite, rutile, biotite, or chlorite. The most common alteration phases comprise chlorite, clay minerals, sericite, sometimes muscovite, calcite, and minerals of the epidote group that generally occur at the plagioclase edges or in tiny grains dispersed inside this mineral or associated with the mafics.

GEOCHEMISTRY

Ten rock samples were selected for the chemical analyses, which were most representative of the Rio Fortuna Gneiss in their spatial distribution and texture diversity. First, these samples were cut, crushed, and pulverized in the Sample Preparation Laboratory of the Mineral Resources Department of the UFMT. Next, the samples were sent to *Acme Analytical Laboratories* (*Acmelab*) Vancouver/Canada for quantifications using ICP (inductively coupled plasma) and ICP-MS (ICP mass spectrometry) methods for major, minor, and trace elements, including rare earth elements (REEs), the results of which are shown in Table 1.

The rocks in this unit are of a slightly expanded acidic nature, with SiO_2 values between 67.17 and 75.76%. The Harker diagrams (Fig. 5) show coherent variation trends, with negative linear correlations between silica and Al_2O_3, $(Fe_2O_3)_t$, MgO, CaO, TiO_2, P_2O_5, and MnO. These characteristics reflect the depletion of calcic plagioclase and primary mafic minerals — such as biotite, titanite, rutile, and apatite — during magmatic evolution. K_2O displays a positive correlation with silica, reflecting the increase in potassic feldspar in the differentiation, whereas the representative points for Na_2O contents in the analyzed rocks yield scattered plots, a result of this element's greater mobility during the action of post-magmatic processes. Among the trace elements, differentiation trends are observed in Sr, V, and Zr, whose distributions and negative correlations with silica are relatively similar, most likely due to the fractionation of plagioclase, titanite, rutile, and zircon.

Geochemically, the rocks studied herein are classified as rhyodacites-dacites and rhyolites in the SiO_2 *versus* Zr/TiO_2 (Fig. 6A; Winchester & Floyd 1977) and alkalis *versus* silica (Fig. 6B; Le Maitre 1989) diagrams and are essentially classified as granodiorites in the diagram proposed by La Roche (1980; Fig. 6C), which considers most major elements (R1 = 4 Si –11 (Na + K) –2 (Fe + Ti) and R2 = 6 Ca + 2 Mg + Al).

The $Na_2O + K_2O$ *versus* SiO_2 diagram of Irvine and Baragar (1971; Fig. 7B) suggests that the magmatism that created the protoliths of the Rio Fortuna Gneiss is of subalkaline affinity, while its calc-alkaline character is made evident in the AFM (Fig. 7A), $Na_2O + K_2O$, and CaO *versus* SiO_2 (Fig. 7B), and La *versus* Yb (Fig. 7C) diagrams proposed by Irvine and Baragar (1971), Peacock (1931), and Barret and MacLean (1999), respectively. The high-K calc-alkaline character of this magmatism is illustrated in Fig. 7D, K_2O *versus* SiO_2 (Le Maitre 2002), and its metaluminous-to-peraluminous affinity is shown in Maniar and Piccoli's A/CNK *versus* A/NK diagram (1989; Fig. 7E).

The tectonic environment was characterized using the Rb *versus* Y + Nb and Hf–Rb–Ta diagrams proposed by Pearce *et al.* (1984; Fig. 8A) and Harris *et al.* (1986; Fig. 8B), respectively. These authors suggest magmatism generated in a magmatic arc. The REE contents of these lithotypes, normalized by Nakamura's chondrite values (1977; Fig. 8C), show similar distributions for most samples, especially for the Light REEs. They also show medium-to-strong fractionation of Heavy REEs in relation to Light REEs, with La/Lu$_N$ values ranging from 8.90 to 50.62 and Eu/Eu* ratios between 0.53 and 1.06. These values correspond to a pattern ranging from moderate to no anomaly. Taken together with the negative Ta and Nb anomalies, this finding reinforces the interpretation that these rocks' origins are related to a magmatic arc environment. Some trace elements other than K_2O in the spidergram shown in Fig. 8D, normalized by the granite values for the Mid-Ocean Ridge by Pearce *et al.* (1984), indicate the enrichment of large-ion lithophile el, especially Rb, Ba, and Th, in relation to the high-field strength elements Ta, Nb, Ce, Hf, Zr, Sm, Y, and Yb. In particular, the existence of a large positive Ce anomaly suggests a likely interaction with seawater (Munhá & Kerrich 1980). Furthermore, except for the Ce element, all high field strength elements display low normalized values (always below 1), which is a typical feature of high-K calc-alkaline magmatism (Scheepers 1995).

STRUCTURAL FRAMEWORK

Studies conducted on the Paraguá Terrane have revealed a complex deformational history for the gneiss and granulite units in Bolivia (Litherland *et al.* 1986; Boger *et al.* 2005) and Brazil (Matos & Ruiz 1991; Ruiz 2005; Figueiredo *et al.*, 2013). The gneiss units in the SBIS are evidence of ductile and ductile-brittle deformation processes and the superposition of at least three deformation phases, which attest to the complex metamorphic and deformational history that affected this unit.

The structural analysis of the Rio Fortuna Gneiss allowed the identification of three deformational phases, from here on denoted as P_1, P_2, and P_3, and their structural elements — folds, foliations, and lineations — which will be, respectively, denoted as Fd, Fl, and L, subscripted with the number of the deformational phase in which they were generated. For example, foliation Fl_1 is generated in the first deformational phase.

First deformational phase (P_1)

The P_1 deformational phase, created by the oldest compressive tectonic effort, was responsible for forming the Fl_1 gneissic banding (Figs. 9A and 11A) defined by the compositional segregation and orientation of the mafic and felsic minerals. The bands range from centimeter to millimeter

Table 1. Chemical composition of major, minor (weight %), and trace elements including REE (ppm) of the Rio Fortuna Gneiss

| Samples	DF-33	DF-33B	DF-33C	DF-38	DF-38A	GJ-19	DF-21	DF-33'	DF-33A'	DF-33B'
Elements										
SiO_2	69.53	71.48	70.66	68.34	67.17	75.76	75.13	69.51	71.57	70.41
Al_2O_3	15.02	13.94	14.29	14.53	14.63	13.79	13.10	15.06	14.17	14.20
MnO	0.06	0.04	0.05	0.05	0.09	0.02	0.02	0.06	0.04	0.05
MgO	0.59	0.63	0.71	1.07	1.91	0.27	0.15	0.61	0.40	0.80
CaO	2.07	1.83	2.09	2.63	3.08	2.69	1.23	2.11	1.42	2.14
Na_2O	3.92	3.13	3.44	3.36	3.52	4.52	3.02	3.91	3.06	3.22
K_2O	4.06	4.61	4.17	3.82	3.82	1.35	4.84	4.13	5.56	4.50
TiO_2	0.42	0.35	0.35	0.60	0.43	0.12	0.21	0.40	0.30	0.44
P_2O_5	0.10	0.10	0.12	0.23	0.21	0.05	0.03	0.11	0.09	0.14
Fe_2O_{3t}	2.85	2.29	2.62	3.75	3.71	0.65	0.98	2.93	1.97	2.79
LOI	1.0	1.2	1.2	1.2	1.1	0.6	1.0	0.8	1.0	0.9
Total	99.66	99.65	99.70	99.58	99.70	99.82	99.74	99.64	99.56	99.98
Ba	1311	1515	1215	1958	994	462.7	660	1422	2240	1578
Nb	5.4	6.6	6.0	10.4	8.9	3.0	9.4	5.4	8.4	9.5
Pb	9.2	9.1	10.8	8.5	13.3	6.6	11.7	8.7	11.0	10.5
Rb	116.6	133.1	139.4	140.7	136.6	41.8	181	124.2	155.8	135.0
Sr	257.7	290.3	262.8	471.5	321.4	270.2	129.7	292.7	247.0	323.9
Th	11.5	10.1	12.9	24.4	10.7	15.9	21.3	13.8	9.2	14.7
U	0.7	0.7	0.7	3.8	1.4	0.8	2.0	0.8	1.4	1.3
V	33	39	38	70	60	5	–	19	34	34
Y	6.7	17.9	16.5	22.8	37.8	13.1	35.6	8.8	27.9	33.2
Zr	305.0	171.5	190.2	211.9	192.5	79.5	132.8	332.1	246.1	228.4
La	61.4	34.1	45.6	41.1	44.0	48.2	54.8	62.5	41.2	43.0
Ce	114.0	71.8	90.1	106.7	86.7	94.9	128.2	126.4	86.3	103.7
Pr	11.47	7.7	9.39	9.84	9.82	9.03	12.83	12.38	9.30	10.33
Nd	39.2	26.4	32.1	36.2	37.5	30.9	46	44.2	36.1	40.4
Sm	4.91	4.87	4.92	5.75	6.40	3.67	7.81	5.32	5.90	7.34
Eu	1.24	1.12	1.17	1.26	1.11	0.80	1.22	1.35	1.42	1.38
Gd	2.81	3.80	3.67	4.57	6.30	2.23	6.12	2.87	4.77	6.15
Tb	0.29	0.61	0.56	0.68	1.03	0.37	1.08	0.36	0.78	1.06
Dy	1.29	3.17	2.91	3.59	6.10	1.77	6.28	1.60	4.38	6.04
Ho	0.20	0.64	0.56	0.79	1.24	0.33	1.29	0.29	0.93	1.21
Er	0.69	1.72	1.77	2.30	3.76	0.89	3.55	0.78	2.65	3.38
Tm	0.10	0.25	0.25	0.37	0.57	0.89	0.54	0.12	0.43	0.52
Yb	0.71	1.49	1.47	2.45	3.41	0.89	3.49	0.85	2.89	3.22
Lu	0.13	0.20	0.22	0.37	0.53	0.12	0.48	0.15	0.45	0.44
Hf	7.9	4.4	5.3	5.9	5.1	2.2	4.3	8.7	6.0	6.1
Ta	0.5	1.1	0.7	1.3	0.7	0.4	1.1	0.5	1.5	1.5
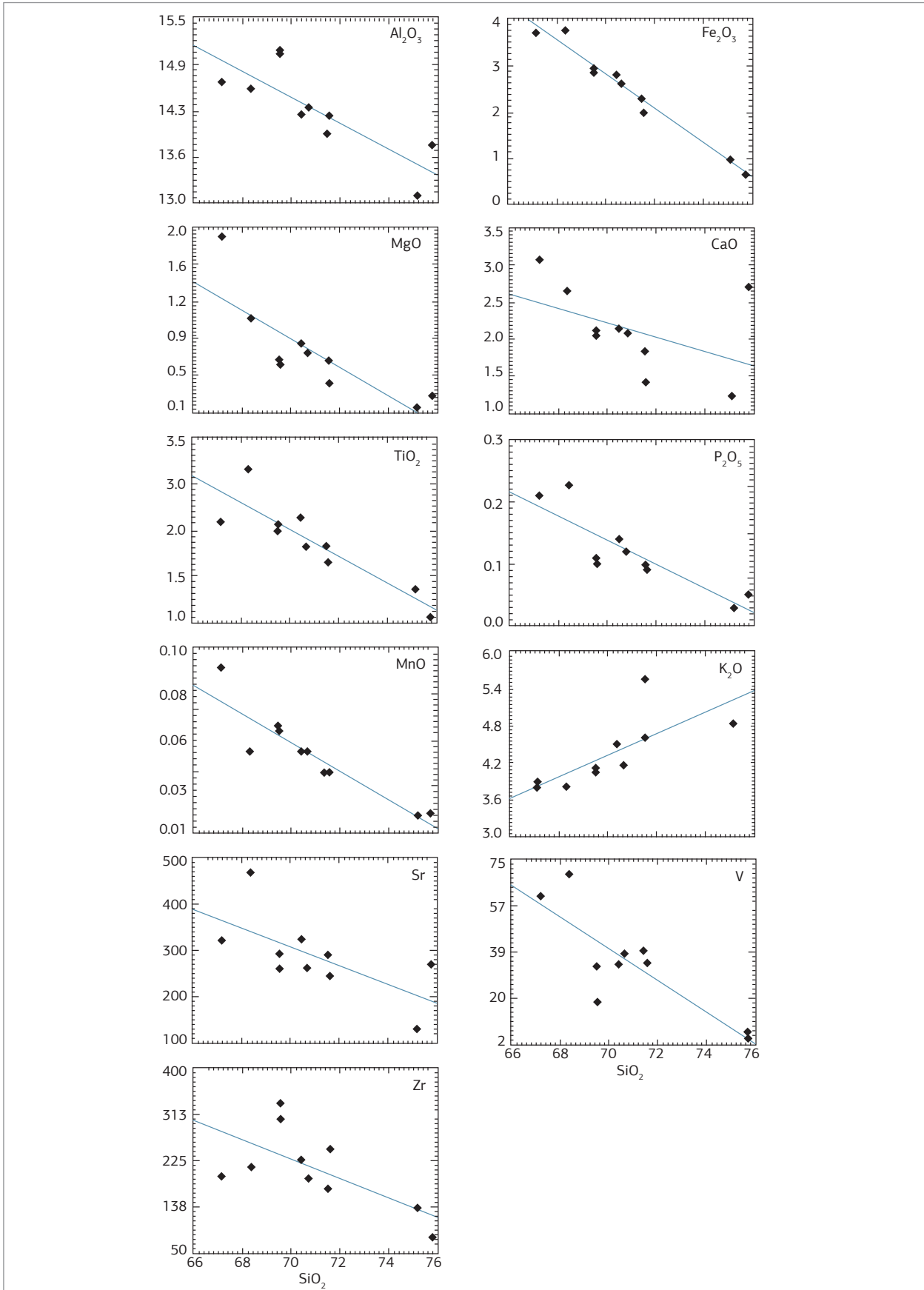
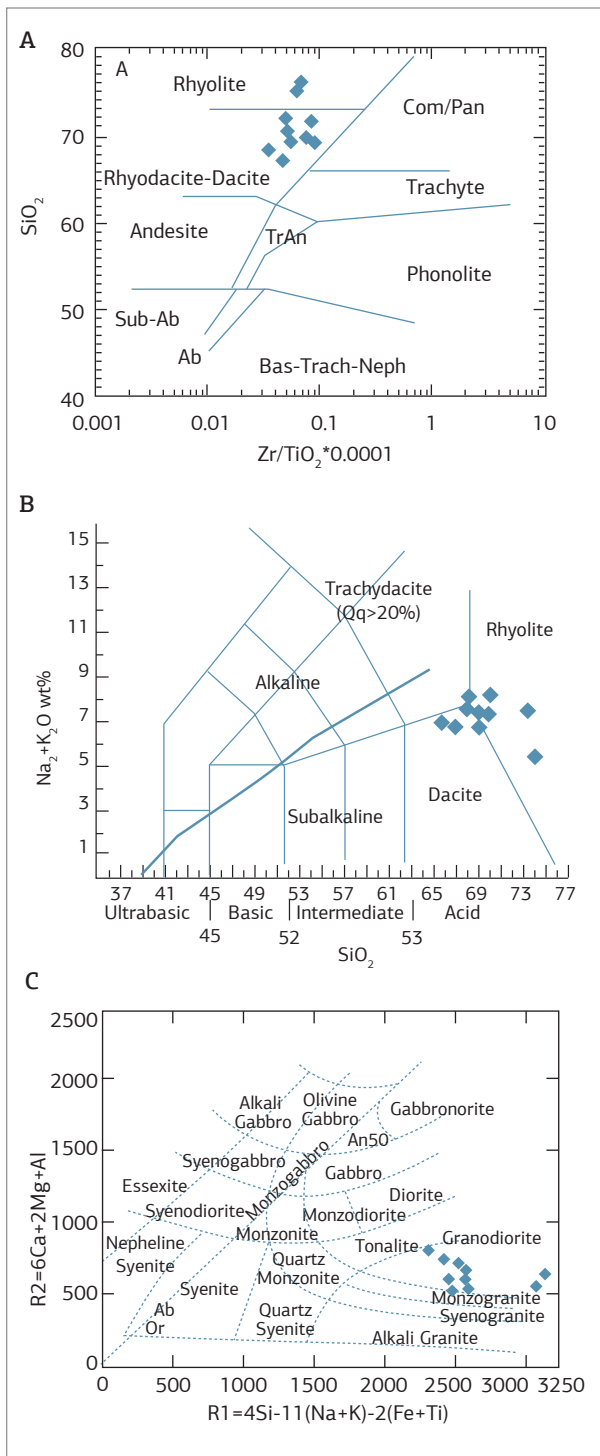Figure 5. Variation diagrams of SiO$_2$ *versus* oxides, with traces for the Rio Fortuna Gneiss.

Figure 6. Classification diagrams for the Rio Fortuna Gneiss rocks: (A) SiO_2 *versus* Zr/TiO_2 (Winchester & Floyd 1977); (B) alkalis *versus* SiO_2 (Le Maitre 1989); (C) R1 *versus* R2 (Le Maitre 1989).

sizes and are discontinuous and irregular. Moreover, a paragenesis constituted by quartz + feldspars + biotites + chlorites + titanites is prominent, and the bands are often found parallel to the younger superimposed Fl_2 foliation.

The gneissic banding's pole stereogram shows a predominant attitude of 40/080 Az and, in a smaller proportion, values close to 250/070 Az (Fig. 11A). The distribution of poles in Fl_1 (Fig. 10A) defines a great circle girdle, indicating the folding of the P_2 phase and the style of the Fd_2 folds, with a slight plunge of the axis towards the NW quadrant.

Second deformational phase (P_2)

Deformational phase P_2 is responsible for the transposition and obliteration of deformational records from the P_1 phase. It is characterized by the tight folds of the Fl_1 foliation and the development of the schistosity-type axial-plane Fl_2 foliation (Fig. 11B). The parageneses found in this metamorphism of the Rio Fortuna Gneiss are mainly composed of hornblende + diopside (rare) + oligoclase, which is indicative of the upper amphibolite facies conditions.

The Fd_2 folds range from centimeter to millimeter sizes, are commonly symmetrical, tight, and of a similar type. Due to the average orientation of the axial surface and the hinge line, the Fd_2 folds are classified as plunging normal folds. At the Fd_2 flanks, it is common to find a transposition of the Fl_1 banding, resulting in parallelism of the Fl_1 and Fl_2 foliations, which display attitudes between 40/080 Az and 70/080 Az (Fig. 10B), with a discrete value scattering. There is also a stretching lineation with an attitude of approximately 35/060 Az associated with the Fl_2 foliation.

Third deformational phase (P_3)

Deformational phase P_3 is marked by the development of the Fl_3 foliation surface (Fig. 11C), which is characterized by the local transposition of the Fl_1 and Fl_2 foliations. Fl_3 is a non-penetrative structure, with a plane axial to the Fd_3 folds, which can be described as open and gentle folds that range from centimeter to millimeter sizes. Fl_3 is classified as an Fl_3 spaced cleavage, commonly associated with discrete zones of ductile shear, with transcurrent kinematics and attitudes varying between 320/085 Az and 005/080 Az.

The crustal reheating imposed on these rocks triggered chemical changes in the alkaline feldspar, plagioclase, and biotite, producing a mineralogical readjustment marked by the formation of the sericite + carbonate + epidote and chlorite paragenesis, representing a paragenesis of green schist facies associated with retrometamorphic features.

U-PB ZIRCON GEOCHRONOLOGY (LA-MC-ICP-MS)

The dated sample from the Rio Fortuna Gneiss (GJ-19) is a leucocratic, light-gray rock that has a medium grain size, is banded, and has a granodioritic composition.
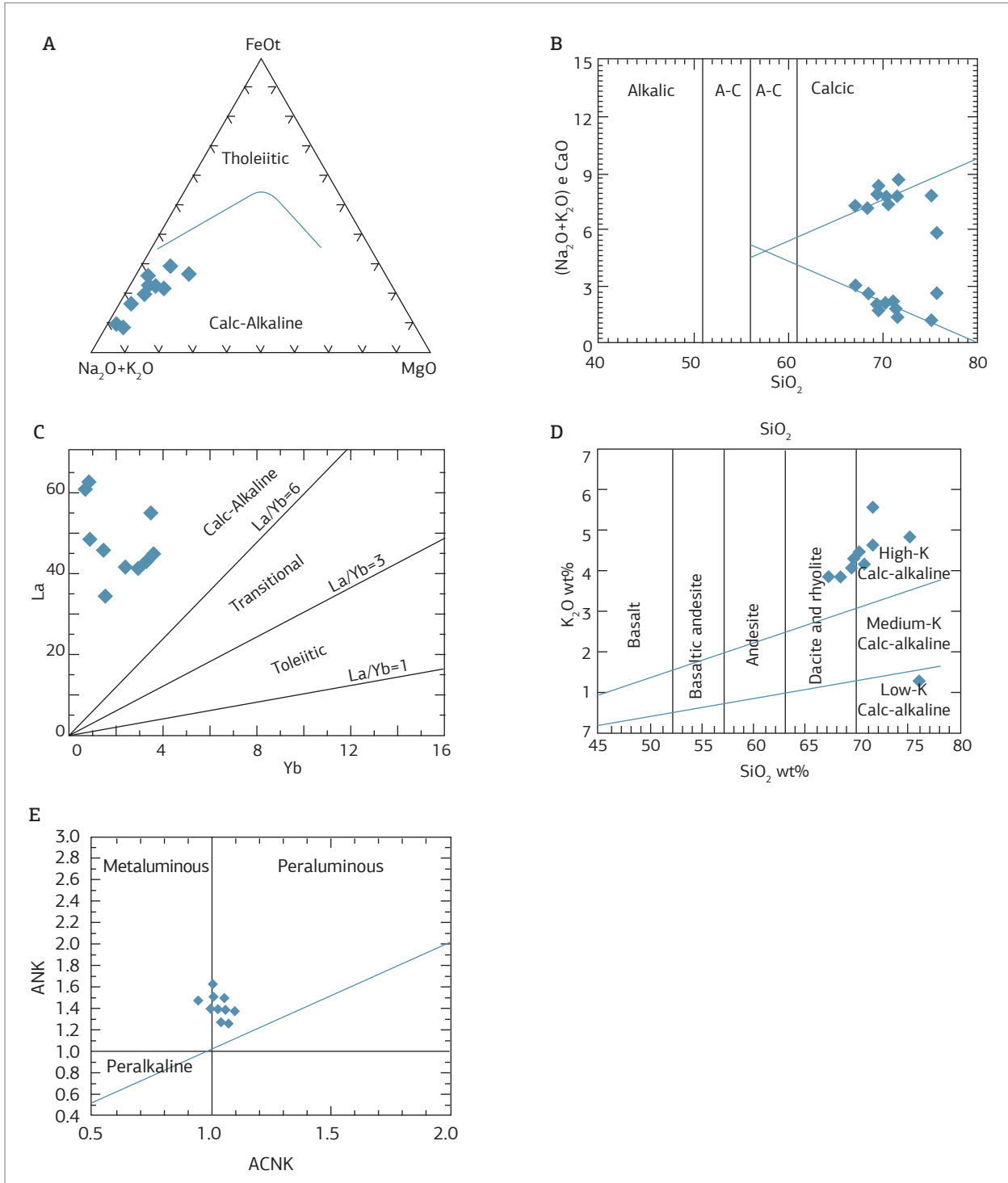
Figure 7. Classification diagrams of magmatic series for the Rio Fortuna Gneiss. (A) AFM (Irvine & Baragar 1971); (B) total alkalis and CaO *versus* silica (Peacock 1931); (C) La *versus* Yb (Barret & MacLean 1999); (D) K$_2$O% *versus* SiO$_2$% (Le Maitre 2002); and (E) A/NK *versus* A/CNK (Maniar & Piccoli 1989).

The zircon crystals analyzed were concentrated in the Sample Preparation Laboratory of the Mineral Resources Department of UFMT. The sample was processed using conventional methods, such as crushing, milling, and sieving. The non-magnetic fraction of the zircon population was separated using the Frantz magnetic separator, and zircon crystals were later manually selected using a binocular stereoscope.
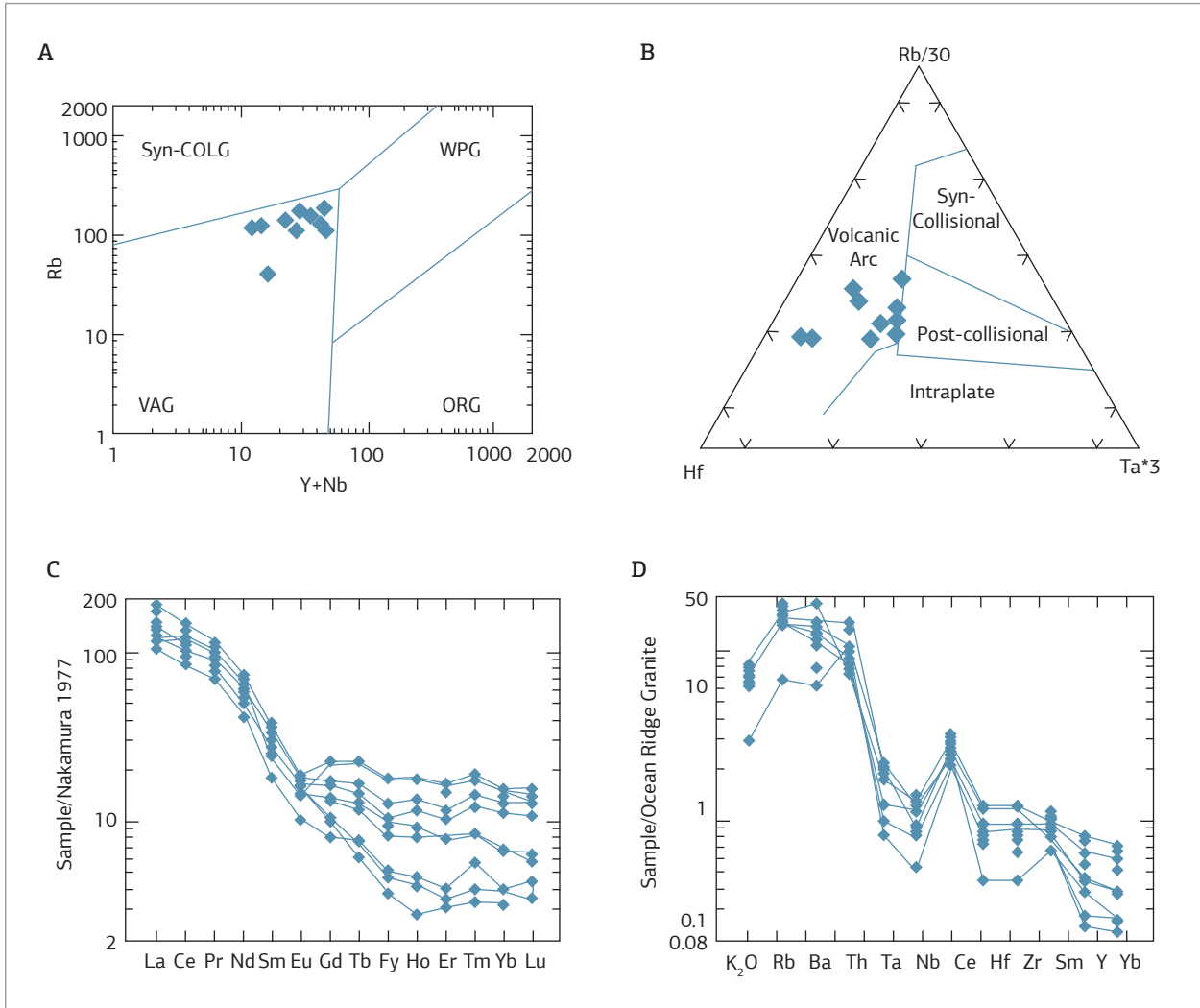
Figure 8. Rio Fortuna Gneiss diagrams: (A) and (B) tectonic environment diagrams, Rb *versus* Y + Nb by Pearce *et al.* (1984) and Hf-Rb-Ta by Harris *et al.* (1986), respectively; (C) REE distribution patterns, normalized by chondrite values (Nakamura 1977); (D) trace elements and K_2O, normalized by the granite values from the Mid-Ocean Ridge (Pearce *et al.* 1984).

Figure 9. Outcrop display the deformations imprinted on the Rio Fortuna Gneiss. Two foliations (Fl1/S1 and Fl2/S2) and the fold Fd2 transposition are prominent.

Crystals were mounted on a disk of epoxy resin, and the section was later polished. Finally, zircon crystals were photographed using scanning electron microscopy (SEM) and conventional optical microscopy (Fig. 13).

Approximately 50 zircon crystals were manually separated (using a binocular stereoscope), of which 14 grains were used to obtain the SEM images and the subsequent analysis. The analyzed zircon crystals were small, yellowish, and range from transparent to opaque; in addition, many of them were broken and fractured.

In the images obtained in the SEM, the zircon grains are characterized by pyramidal faces and terminations, and there are small fractures perpendicular to the faces in some of the grains (Fig. 12A, 12C, and 12E). Zircons A and E are rounder and have inclusions and fractures; in addition, clear zoning can be identified. The zircon crystal shown in Fig. 12C is more prismatic, and its zoning is not so evident.
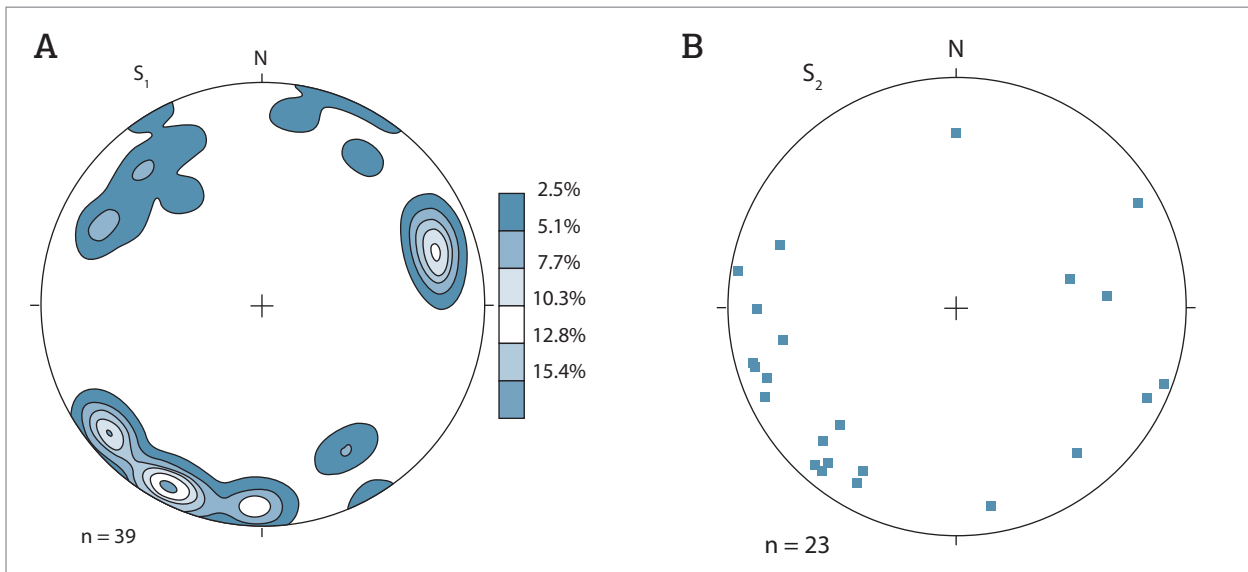
Figure 10. (A) Isofrequency stereogram for the Fl_1 gneiss banding's poles, illustrating the great circle girdle distribution caused by the folds of the P_2 phase, and (B) stereogram of the pole points of the Fl_2 schistosity.
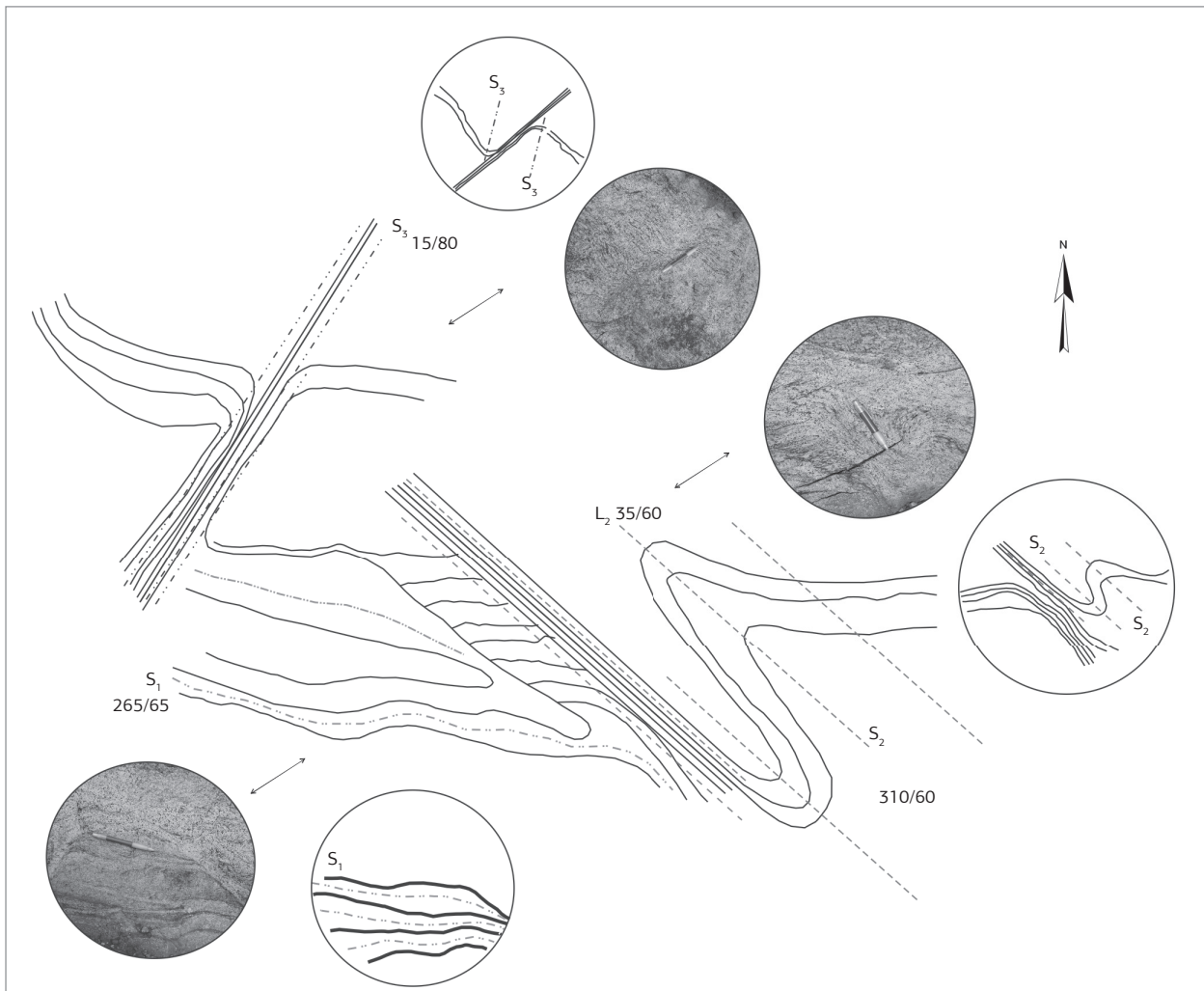

Figure 11. Illustrative schema for the deformational phases that affect the Rio Fortuna Gneiss. (A) Gneiss banding highlighting the non-transposed first foliation (Fl_1); (B) Fl_1 gneissic banding folded and partially transposed according to the direction of the Fl_2 foliation; and (C) transposition of the Fl_1 and Fl_2 foliations along the narrow shearing zones parallel to the Fl_3 foliation.

The analytical data with the isotopic ratios for the crystals dated using the U-Pb method are presented in Tab. 2. Isotope analyses were conducted in the Isotopic Geology Laboratory of the Federal University of Rio Grande do Sul (Universidade Federal do Rio Grande do Sul) using a Thermo-Finnigan "Neptune" multicollector mass spectrometer with ICP and a "New Wave" laser ablation system (LA-MC-ICP-MS). After point analysis, the data were treated using proprietary software developed by Thermo-Finningan.

The concordia diagram obtained with the Isoplot v.3 software application (Ludwig 2001) shows that the zircon crystals analyzed herein provide an age for the upper intercept (forced through the origin) of 1,711 ± 13 Ma (Fig. 13). This result most likely corresponds to the crystallization age of the igneous protolith, and it is close to the youngest results published by Santos *et al.* (2008), between 1,772 and 1,734 Ma, obtained from the core portions of the zircon crystals of the same body studied herein.
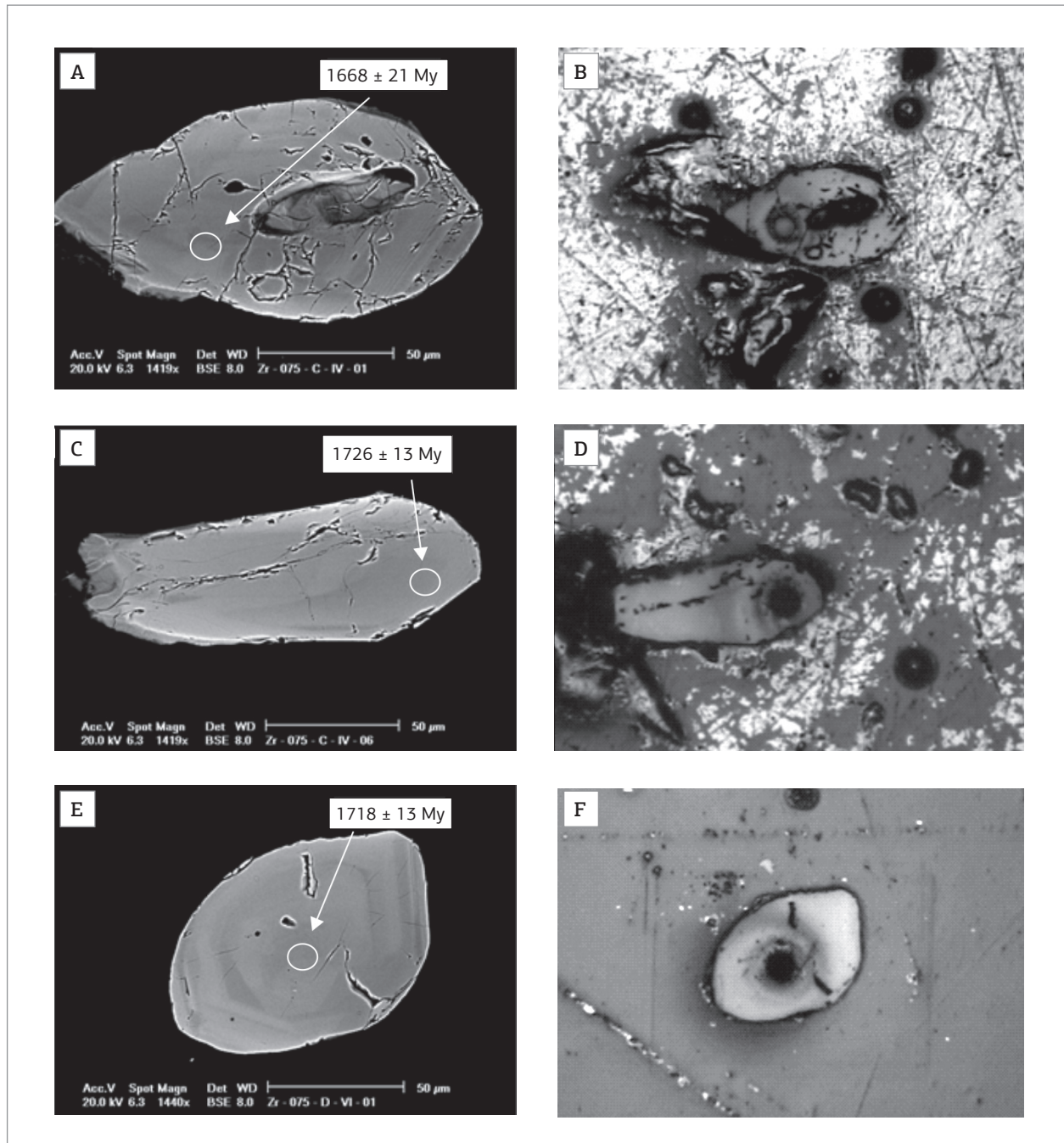

Figure 12. SEM images and optical microscopy photographs of the zircon crystals, with 25 μm spots produced by the laser microprobe, where A and B = Zr-075-C-IV-01, C and D = Zr-075-C-IV-06, and E and F = Zr-075-D-VI-01.

Table 2. Synthesis of the data obtained from the U/Pb analysis on zircon using LA-MC-ICP-MS for the GJ-19 sample

N° Spot	Concórdia 1					Concórdia 2				
	$^{207}Pb/^{235}U$	±	$^{206}Pb/^{238}U$	±	Rho	$^{238}U/^{206}Pb$	±	$^{207}Pb/^{206}U$	±	Rho
Zr-075-C-IV-01	4.1635	2.57	0.2936	2.01	0.78	3.4058	2.01	0.1028	1.61	1.25
Zr-075-C-IV-02	4.2951	2.02	0.2892	1.17	0.58	3.4578	1.17	0.1077	1.65	0.71
Zr-075-C-IV-05	4.5309	2.03	0.3153	0.94	0.46	3.1719	0.94	0.1042	1.80	0.52
Zr-075-C-IV-06	4.4780	1.51	0.3084	1.18	0.78	3.2427	1.18	0.1053	0.94	1.25
Zr-075-C-IV-10	4.7639	1.40	0.3045	1.05	0.75	3.0604	1.05	0.1057	0.92	1.14
Zr-075-C-IV-15	4.3726	2.22	0.3268	1.37	0.62	3.2838	1.37	0.1041	1.75	0.78
Zr-075-D-V-01	4.9488	1.52	0.3406	0.72	0.47	2.9360	0.72	0.1054	1.34	0.53
Zr-075-D-V-02	4.7954	1.37	0.3305	0.74	0.55	3.0254	0.74	0.1052	1.14	0.65
Zr-075-D-V-04	4.6649	1.21	0.3232	0.83	0.69	3.0938	0.83	0.1047	0.88	0.95
Zr-075-D-V-10	4.6879	1.59	0.3254	1.03	0.66	3.0731	1.04	0.1045	1.20	0.87
Zr-075-C-VI-01	4.3907	1.75	0.3072	1.01	0.58	3.2554	1.01	0.1037	1.43	0.71
Zr-075-C-VI-04	4.7747	1.60	0.3298	0.98	0.61	3.0320	0.98	0.1050	1.26	0.77
Zr-075-C-VI-06	4.5419	1.82	0.3142	1.30	0.71	3.1827	1.30	0.1048	1.27	1.02

| N° Spot	Age (Ma)					$^{23}Th/^{23}U$	% Discor.	f206
	$^{207}Pb/^{235}U$	±	$^{207}Pb/^{235}U$	$^{207}Pb/^{206}U$	±			
Zr-075-C-IV-01	1660	33	1667	1676	27	0.7219	1	0.0002
Zr-075-C-IV-02	1638	19	1692	1761	29	0.4752	7	0.0004
Zr-075-C-IV-05	1767	17	1737	1701	31	0.8895	-4	0.0018
Zr-075-C-IV-06	1733	21	1727	1720	16	0.5508	-1	0.0000
Zr-075-C-IV-10	1823	19	1779	1727	16	0.6541	-6	0.0002
Zr-075-C-IV-15	1714	24	1707	1699	30	0.7014	-1	0.0008
Zr-075-D-V-01	1890	14	1811	1721	23	0.8015	-10	0.0012
Zr-075-D-V-02	1841	14	1784	1718	20	0.4998	-7	0.0001
Zr-075-D-V-04	1805	15	1761	1709	15	0.9142	-6	0.0003
Zr-075-D-V-10	1816	19	1765	1705	20	0.5539	-6	0.0004
Zr-075-C-VI-01	1727	18	1711	1691	24	0.5148	-2	0.0030
Zr-075-C-VI-04	1937	18	1780	1714	22	0.7106	-7	0.0001
Zr-075-C-VI-06	1761	23	1739	1712	22	0.5699	-3	0.0002

DISCUSSION AND FINAL REMARKS

The SW portion of the Amazonian Craton developed by the successive joining of terranes, which culminated with the formation of the Rodinia Supercontinent (Boger *et al.* 2005; Bettencourt *et al.* 2010, among others). The Paraguá Terrane, considered within this study as an allochthonous continental block, exhibits geological records that indicate a polycyclic evolution history of long duration. The oldest geological units are paleoproterozoic and the youngest are neoproterozoic.

The Rio Fortuna Gneiss consists of ortho-derived, monzogranitic to granodioritic rocks of light-gray color and medium-to-fine grain size, and the formation exhibits a prominent banded structure, a polydeformed pattern, and, quite often, partially assimilated and stretched amphibolite xenoliths. Felsic beds alternate with dark, discontinuous bands of millimeter size, whose predominant mafic mineral is biotite and which have a sagenitic texture. The accessory minerals are represented by titanite, rutile, allanite, apatite, and opaques, whereas chlorite, sericite, muscovite, epidote/clinozoisite, clay minerals, calcite, and another generation of titanite and opaques make up the alteration paragenesis.

Regarding the deformational history, the gneiss studied herein shows records of at least three deformational phases associated with the orogenies that affected the Paraguá Terrane. The P_1 deformational phase, characterized by the generation of the
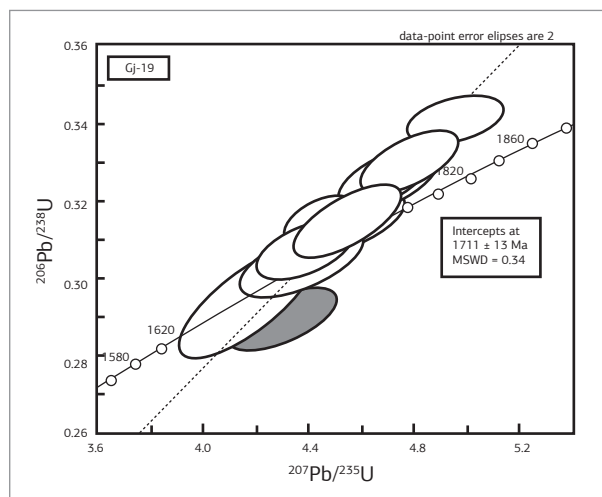
Figure 13. U-Pb concordia diagram for the GJ 19 sample from the Rio Fortuna Gneiss. The age obtained for the upper intercept is 1,711 ± 13 Ma.

gneissic banding (Fl_1) at the deep crustal level, has been intensely affected by the P_2 deformational phase. This new phase triggers the transposition of the Fl_1 banding, which takes on a predominant attitude of 40/080 Az or 250/80 Az, and nucleates symmetric, closed, and similar-type folds with flank transposition. The Fl_2 foliation, arranged according to the axial surface of the Fd_2 folds, is characterized as a schistosity with an attitude between 40/080 Az and 70/080 Az. The P_3 deformational phase is marked by the appearance of the Fl_3 foliation, which is characterized by locally transposing the Fl_1 and Fl_2 foliations according to an average direction of 150/80 Az. Furthermore, it is not penetrative and is associated with open and gentle folds (Fd_3).

Tentatively, the structures formed in P_1 are related to the oldest orogenic event, most likely the Lomas Manechis Orogeny from Litherland *et al.* (1986) and Bettencourt *et al.* (2010). The P_2 phase creates tectonic structures that can be correlated with the structural elements described in the sin- to tardi-kinematic granitoids of the Pensamiento Intrusive Suite (1.36 – 1.30 Ga.), which allows this deformational phase to be associated with the San Ignácio Orogeny from Litherland *et al.* (1986). The last phase (P_3) occurred in a shallow crustal level, as indicated by the ductile-brittle structures described herein. However, it was not possible, based on the data obtained in this study, to propose their association to any of these orogenic events.

Geochemically, these rocks are an acidic sequence formed by subalkaline magmatism of the high-potassium calc-alkaline type, from peraluminous to metaluminous, which evolved through fractionated crystallization mechanisms associated with crustal contamination. The U/Pb zircon geochronological data indicate 1,711 ± 13 Ma to be the crystallization age of the lithotype studied here.

The geological, geochemical, and geochronological data obtained for the Rio Fortuna Gneiss are comparable to those of the Chiquitania Gneiss complex of Litherland *et al.* (1986) and, more exactly, to those from Unit B gneisses. From the tectonic environment perspective, the results in this study suggest that the igneous protolith was generated in a convergent tectonic environment, similar to the continental magmatic arc, of andine-type due to the consumption of the paleoproterozoic oceanic lithosphere. The polydeformed character of the Rio Fortuna Gneiss, in association with the U-Pb age of 1,336 ± 6 Ma obtained at the edge of a zoned zircon (Santos *et al.* 2008), suggests that it suffered the same metamorphic and deformational effects of the San Ignácio Orogeny, possibly the event marking the joining of the Paraguá Terrane to the Amazonian proto-craton. The last tectonic event, i.e., the Sunsás Orogeny, weakly reworks the Rio Fortuna Gneiss rocks, as well as those from other geological units in the paleo- to mesoproterozoic basement.

REFERENCES

Barrett T.J. & MacLean W.H. 1999. Volcanic sequences, lithogeochemistry, and hidrothermal alteration in some bimodal volcanic-associated massive sulfide systems. *Reviews in Economic Geology*, **8**:101-131.

Bettencourt J.S., Leite Jr. W.B., Ruiz A.S., Matos R., Payolla B.L., Tosdal R.M. 2010. The Rondonian-San Ignácio Province in the SW Amazonian Craton: An overview. *Journal of South American Earth Sciences*, **29**(1):28-46.

Boger S.D., Raetz M., Giles D., Etchart E., Fanning C.M. 2005. U-Pb age data from the Sunsas region of Eastern Bolivia, evidence for the allochthonous origin of the Paragua Block. *Precambrian Research*, **139**: 121-146.

Cox K.G., Bell J.D., Pankhurst R.J. 1979. The interpretation of igneous rocks. George, Allen e Unwin, London.

Faria D.A. 2011. Geologia, geoquímica e geocronologia da Suíte Intrusiva Serra do Baú-Ênfase no gnaisse Rio Fortuna-Terreno Paraguá, SW do Craton Amazônico-Brasil. Dissertação de Mestrado. Instituto de Ciências Exatas e da Terra, Universidade Federal do Mato Grosso, p. 92.

Figueiredo F.L.P., Ruiz, A.S., Sousa, M.Z.A. de, Macambira, M.J.B. 2013. Ortognaisse Turvo – registro de magmatismo Paleoproterozóico no Terreno Paraguá - SW do Cráton Amazônico. *Brazilian Journal of Geology*, **43**(2):401-422.

Harris N.B.W., Pearce J.A., Tindal A.G. 1986. Geochemical characteristics of collision-zone magmatism. *In*: M.P. Coward & A.C. Ries (ed.), Collision Tectonics, London. *The Geological Society Special Bulletin*, **19**:67-81.

Geraldes M.C. 2000. Geocronologia e geoquímica do Plutonismo Mesoproterozóico do SW do Estado de Mato Grosso (SW do Cráton Amazônico). Instituto de Geociências, Universidade de São Paulo, São Paulo, Ph.D Thesis, p. 193.

Irvine T.N. & Baragar W.R.A. 1971. A guide to the chemical classification of the common volcanic rocks. *Canadian Journal of Earth Sciences*, **8**:523-548.

La Roche (de) H. 1980. Granites chemistry through multicationic diagrams. *Sciences de la Terre, Série Informatique Géologique*, **13**:65-88.

Le Maitre R.W.A. 1989. *Classification of Igneous Rocks and Glossary of Terms*: Recommendations of the International Union of Geological-Sciences Subcommission on the Systematics of Igneous Rocks. Oxford, Blackwell, p. 193.

Le Maitre R.W. 2002. *Igneous Rocks: A Classification and Glossary of Terms*: Recommendations of the International Union of Geological Sciences Subcommission on the Systematics of Igneous Rocks. Cambridge, Cambridge University Press, p. 236.

Litherland M., Annells R.N., Appleton J.D., Berrangé J.P., Bloomfield K., Burton C.C.J., Darbyshire D.P.F., Fletcher C.J.N., Hawkins M.P., Klinck B.A., Lanos A., Mithcell W.I., O Connor E.A., Pitfield P.E.J., Power G.E., Webb B.C. 1986. *The Geology and Mineral Resources of the Bolivian Precambrian Shield*. British Geological Survey. Overseas Memoir 9. London, Her Majesty's Stationery Office. p. 140.

Ludwig K.R. 2001. ISOPLOT/Ex. rev., 2.49. A geochronological toolkit for Microsoft Excel. Berkeley Geochronological Center, Special Publication 1A, p. 59.

Maniar P.D. & Piccoli P.M. 1989. Tectonic discrimination of granitoids. *Geological Society American Bulletin*, **101**:635-643.

Matos J.B. & Ruiz A.S. 1991. Contribuição à geologia da Folha Santa Rita [Contribution to the geology of the Santa Rita sheet] – Mato Grosso. *In*: III Simp. Geol. Centro Oeste, Proceedings, Cuiabá, p. 122-130.

Matos J.B., Sousa M.Z.A., Silva C.H., Costa P.C.C., Ruiz A.S., Quadros A.P., Godoy A.M., Assis M.M.C., Jesus G.C. 2006. O Ortognaisse Tarumã do Domínio Paraguá: Caracterização petrogenética preliminar. *In*: IX Simp. Geol. Centro Oeste, Proceedings, Goiânia, p. 187-190.

Matos R., Teixeira W., Geraldes M.C., Bettencourt J.S. 2009. *Geochemistry and Nd-Sr Isotopic Signatures of the Pensamiento Granitoid Complex, Rondonian-San Ignacio Province, East Precambrian Shield of Bolívia: Petrogenetic Constraints for a Mesoproterozoic Magmatic Arc Setting*. Geol. USP, Sér. Cient., São Paulo, **9**(2):89-117.

Munhá J. & Kerrich R. 1980. Sea water-basalt interaction in spilites from the Iberian Pyrite Belt; Contributions to Mineralogy and Petrology, v. 73, p. 191-200.

Nakamura K. 1977. Volcanoes as a possible indicator of tectonic stress orientation: Principle and proposal. *Journal of Volcanology and Geothermal Research*, **2**:1-16.

Peacock M.A. 1931. Classification of igneous rock series. *Journal of Geology*, **39**:54-67.

Pearce J.A., Harris N.B.W., Tindle A.G. 1984. Trace element discrimination diagrams for the tectonic interpretation of granitic rocks. *Journal of Petroleum*, **25**(4):956-983.

Ruiz A.S. 2005. Evolução geológica do Sudoeste do Cráton Amazônico Região Limítrofe Brasil-Bolívia-Mato Grosso. UNESP. Rio Claro, SP. Ph.D Thesis, p. 260.

Ruiz A.S. 2009. Compartimentação tectônica (Pré-Sunsás) do SW do Cráton Amazônico: ênfase em Mato Grosso – Brasil. *In*: XVIII Congresso Geológico Boliviano, Potosi, Proceedings.

Saes G.S. 1999. Evoluão tectônica e paleogeográfica do Aulacogeno Aguapeí (1.2 - 1.0 Ga) e dos Terrenos do seu embasamento na Porção Sul do Cráton Amazônico. Geosciences Institute, University of São Paulo, Ph.D Thesis, p. 135.

Santos J.O.S., Hartmann L.A., Gaudette H.E., Groves D.I., Mcnaughton N.J., Fletcher I.R.A. 2000. New understanding of the provinces of the Amazon Craton based on integration of field mapping and U-Pb and Sm-Nd geochronology. *Gondwana Research*, **3**(4):453-488.

Santos J.O.S., Rizzotto G.J., Potter P.E., Mcnaughton N.J., Mato R.S., Hartmann L.A., Chemale Jr. F., Quadros M.E.S. 2008. Age and autochthonous evolution of the Sunsás Orogen in the West Amazon Craton based on mapping and U-Pb geochronology. *Precambrian Research*, **165**:120-152.

Scheepers R. 1995. Geology, geochemistry and petrogenesis of Late Precambrian S-, I- and A- type granitoids in the Saldania belt, Western Cape Province, South Africa. *Journal of African Earth Sciences*, **21**(1):35-58.

Streckeisen A. 1976. *To each plutonic rock, its proper name*. Earth Science Review, Amsterdam, v. 12, p. 1-33.

Tassinari C.C.G. & Macambira M.J.B. 1999. Geochronological provinces of the Amazonian Craton. Episodes **22**, 174-182.

Tassinari C.C.G., Bettencourt J.S., Geraldes M.C., Macambira M.J.B., Lafon J.M. 2000. The Amazonian Craton. *In*: Cordani U.G., Milani E.J., Thomaz Filho A., Campos D.A. (eds.), Tectonic evolution of South America. *31st International Geological Congress*, Rio de Janeiro, Brazil, p. 41-95.

Teixeira W., Tassinari C.C.G., Cordani U.G., Kawashita K. 1989. A review of the geochronology of the Amazonian Craton: Tectonic implications. *Precambrian Research*, **42**:213-227.

Winchester J.A. & Floyd P.A. 1977. Geochemical discrimination of different magma series and their differentiation products using immobile elements. *Chemical Geology*, **20**:325-343.